Chaos, Solitons and Fractals 188 (2024) 115573

Contents lists available at ScienceDirect

Chaos, Solitons and Fractals

journal homepage: www.elsevier.com/locate/chaos

Recurrent nonlinear modulational instability in the β-FPUT chain

Andrea Armaroli *, Stefano Trillo

Department of Engineering, University of Ferrara, via Saragat, 1, 44121, Ferrara, Italy

ARTICLE INFO

Keywords:
Modulational instability
Fermi-Pasta-Ulam-Tsingou recurrence
Nonlinear Schrödinger equation
Regular motion

ABSTRACT

We address the fully nonlinear stage of seeded modulational instability in the Fermi-Pasta–Ulam-Tsingou chain with quartic interaction potential (β-FPUT) subject to periodic boundary conditions. In particular, we investigate quantitatively the validity of the continuous approximation that describes the evolution of a narrow band of normal modes in terms of the ubiquitous nonlinear Schrödinger equation (NLSE) or its generalizations. By injecting three normal modes comprising a pair of unstable sidebands, we find that the FPUT chain exhibits, for weak enough nonlinear interaction, recurrent evolutions (though of different nature compared with the original work by FPUT). Such recurrences generally preserve the homoclinic structure of nonlinear modulational instability ruled by the NLSE, with generated higher order-modes being essentially enslaved to the unstable pair. Under some circumstance, we find that pseudo-random separatrix crossing events may occur even for a very weak interaction strength.

1. Introduction

Since the pioneering studies of modulational instability (MI) [1] or Benjamin-Feir instability [2], i.e., the destabilization of a homogeneous wave (also denoted as pump or background) subject to harmonic perturbations (see [3] for a historical perspective), it turns out that the simplest model to describe the nonlinear dynamics after the initial exponential growth of the perturbations is the ubiquitous nonlinear Schrödinger equation (NLSE) [4]. This has become one of the most studied models in nonlinear physics, because it applies to many different settings: unidirectional surface gravity waves in the ocean, propagation of short pulses in monomode optical fibers, Langmuir plasma waves, and coherent matter waves in Bose–Einstein condensates of ultracold atoms, to name only a few. Furthermore its well-known integrability property guarantees that its solutions are regular and relatively simple, as in the cases (all related to MI) of Akhmediev breathers (ABs) [5,6], its Peregrine soliton limit [7], or doubly periodic solutions [6,8], and hence suit naturally to the description of laboratory and numerical experiments.

A major problem that attracted a lot of interest since the early experiments on MI stimulated by the injection of unstable sideband modes [9] is the fully nonlinear or depleted stage of the evolution beyond the initial exponential growth of the harmonic perturbation. This yields the formation of a pulse train which often has been interpreted in terms of generation of a soliton train with repetition rate fixed by the unstable seeded frequency [10,11]. However, this turns out a naive argument, since, over the long-term dynamics, the nonlinear MI ruled by the NLSE exhibits cycles of conversion and back-conversion between the homogeneous wave and multiple sideband harmonic modes (first noticed in [9]), which globally results into a recurrent (periodic or quasi-periodic) evolution[12–18]. Such recurrences are organized according to a homoclinic phase-plane structure which, despite involving infinitely many sideband modes, essentially resembles that of a low-dimensional [1 degree of freedom (d.o.f.)] oscillator [6,19]. In particular nonlinear optics has recently proved a formidable and flexible ground for the observation of such phase-space structure [14–17], whereas the solution of the NLSE initial value problem associated with the excitation of few modes provide simple yet accurate formulas to describe the recurrent MI evolutions [20,21].

We also recall that similar phase-space structures is ubiquitous [22] and not limited to integrable models [23,24].

In this context, it has become somehow natural and widespread to refer (after Ref. [9]) to recurrent nonlinear MI as a manifestation of the celebrated Fermi-Pasta–Ulam-Tsingou (FPUT) paradox [25] in different areas, ranging from hydrodynamics [13] and optics [12,14,15, 26,27], to nonlinear physics [28–31]. The FPUT paradox consists in the pioneering observation that the energy initially launched in the lowest-order frequency normal mode of a nonlinear chain flows back to it after coupling to higher frequency modes, instead of being equipartitioned between all modes as expected by Fermi and coworkers. The FPUT

* Corresponding author.
E-mail address: andrea.armaroli@unife.it (A. Armaroli).

https://doi.org/10.1016/j.chaos.2024.115573
Received 4 July 2024; Received in revised form 20 September 2024; Accepted 21 September 2024
Available online 30 September 2024
0960-0779/© 2024 The Authors. Published by Elsevier Ltd. This is an open access article under the CC BY-NC-ND license (http://creativecommons.org/licenses/by-nc-nd/4.0/).

recurrence is at the origin of several major discoveries in nonlinear science reviewed in [32–36], the testbed for new mathematical ideas [37–40], and still represents a topic of very active research [41–44].

It can be argued that the original FPUT recurrence and the nonlinear MI differ in several key respects such as the discrete versus continuous nature of the two models, and the type of excitation (lowest frequency mode in FPUT chains versus a generic pump mode and its modulating adjacent sideband modes in the NLSE). However, in our opinion, this does not prevent to consider nonlinear MI as a FPUT phenomenon if the latter is intended in a broader sense than the original FPUT result. Rather, what seems to be missing is a systematic attempt to connect quantitatively the recurrences of the nonlinear MI ruled by the NLSE to possibly similar dynamics in the real FPUT chain. This is the aim of the present paper.

Indeed, if a FPUT chain with quartic interaction known as β-FPUT is considered, it can be shown that the evolution of a narrow packet of modes can be approximated by the NLSE [45]. So far, the NLSE limit was exploited to estimate through its conservations the so called *stochasticity threshold*, above which the energy exchange between modes is irregular, i.e., in modern terms, chaotic. While Hamiltonian chaos is expected to occur in the FPUT system for very long integration times, we stress that the NLSE is integrable, thus cannot rigorously behave chaotically.

Here we are rather interested, keeping nonlinear MI in mind, to quantitatively compare the true FPUT evolutions with their NLSE approximation. Thanks to the cornucopia of results obtained in the last 50 years on the latter, the comparison can be put on a rigorous ground, allowing us to understand in which regimes the FPUT exhibits a nontrivial dynamics nearly indistinguishable from the NLSE or, viceversa, where this comparison is less rigorous and leads to deviations between the two models.

First, we consider an initial condition composed of three modes at the edge of the Brillouin zone (the highest frequency). Most of the previous studies of energy conversion from high to low energy (frequency) modes (at variance with the original FPUT work and sometimes referred to as anti-FPUT problem), see [46–51], were focused on the route to thermalization and the mediating role of so-called chaotic breathers. Here we consider instead a weak enough nonlinearity and study the correspondence between FPUT and NLSE solutions for a single modulationally unstable mode, the dynamics of which is equivalent to a single degree of freedom (d.o.f.) Hamiltonian with double well potential [14,19,52]. The comparison to a more rigorous perturbation theory based on finite-gap method [20,21,53] allows us to quantify the discrepancy between the NLSE and true FPUT dynamics. Both approaches highlight the role of the AB, a spatially periodic breather of completely different nature compared with so-called q-breathers [40] or chaotic breathers [33], as the homoclinic orbit that divide qualitatively different types of recurrent dynamics.

We address also the case of a wave-packet not centered around the edge of the Brillouin zone, and find that higher-order terms must be included to generalize the NLSE. We limit ourselves to terms similar to 4th-order propagation models of water surface gravity waves [54,55]. The effect of the resulting terms [34] on MI is absent, but the subsequent nonlinear evolution exhibits a linear shift in space with respect to the frame moving at the group velocity of the packet center. This phenomenon can be explained as a perturbation of the NLSE dynamics.

We finally find that the FPUT evolution may differ from the NLSE regular orbits, notably alternating pseudo-stochastically between the two wells. We limit ourselves to present numerical evidence for this phenomenon, leaving a quantitative explanation, which likely requires a more sophisticated perturbation theory, for future developments.

After recalling the derivation of a generalized NLSE from the β-FPUT system (Section 2), we present and discuss several detailed numerical simulations (Section 3), before presenting our conclusions and perspectives in Section 4.

2. Analytical model

We consider here the β-FPUT Hamiltonian

$$H(u_n,p_n)=\sum_{n=0}^{N-1}\frac{p_n^2}{2}+\frac{1}{2}\left(u_{n+1}-u_n\right)^2+\frac{\beta}{4}\left(u_{n+1}-u_n\right)^4 \tag{1}$$

By writing the Hamilton equations, $\dot{u}_n=\frac{\partial H}{\partial p_n}$, $\dot{p}_n=-\frac{\partial H}{\partial u_n}$, we obtain

$$\ddot{u}_n=u_{n+1}+u_{n-1}-2u_n+\beta\left[\left(u_{n+1}-u_n\right)^3-\left(u_n-u_{n-1}\right)^3\right]. \tag{2}$$

We assume periodic boundary conditions $u_0=u_N$, $p_0=p_N$. It is well known, see for example [45,56], that, defining the variables (amplitudes of normal modes)

$$a_k\equiv\frac{1}{\left(2\omega_k\right)^{\frac{1}{2}}}\left(P_k-i\omega_k U_k^*\right), \tag{3}$$

with $k=0,\dots,N-1$, $\omega_k=2\sin\frac{\pi k}{N}$, $P_k\equiv\frac{1}{N^{\frac{1}{2}}}\sum_{n=0}^{N-1}p_n e^{i\frac{2\pi k}{N}n}$ and $U_k\equiv\frac{1}{N^{\frac{1}{2}}}\sum_{n=0}^{N-1}u_n e^{-i\frac{2\pi k}{N}n}$, the system is still in canonical form and the interaction terms are quartic. The Hamiltonian reads

$$\begin{aligned}H(a_k,a_k^*)=&\underbrace{\sum_{k=0}^{N-1}\omega_k a_k a_k^*}_{\text{lin.}}\\&+\frac{1}{2}\sum_{k_1,k_2,k_3,k_4=0}^{N-1}T_{1,2,3,4}\Bigg(\underbrace{a_{k_1}^*a_{k_2}^*a_{k_3}a_{k_4}\delta_{1,2}^{3,4}}_{2\to2,\text{ res.}}\\&+\underbrace{\frac{1}{3}a_1^*a_{k_2}a_{k_3}a_{k_4}\delta_1^{2,3,4}}_{1\to3,\text{ non-res.}}+\underbrace{a_{k_1}^*a_{k_2}^*a_{k_3}^*a_{k_4}\delta_{1,2,3}^4}_{3\to1,\text{ non-res.}}\\&+\underbrace{\frac{1}{3}a_{k_1}^*a_{k_2}^*a_{k_3}^*a_{k_4}^*\delta_{1,2,3,4}}_{4\to0,\text{ non-res.}}\Bigg),\end{aligned} \tag{4}$$

with $\delta_1^{2,3,4}\equiv\delta(k_1-k_2-k_3-k_4)$, $\delta_{1,2}^{3,4}\equiv\delta(k_1+k_2-k_3-k_4)$, etc…

The nonlinear tensor reads

$$T_{1,2,3,4}\equiv\frac{3\beta}{4N}\mathrm{sgn}(k_1k_2k_3k_4)\left[\omega_{k_1}\omega_{k_2}\omega_{k_3}\omega_{k_4}\right]^{\frac{1}{2}}. \tag{5}$$

In Eq. (4), we wrote all the nonlinear terms, separating resonant from non-resonant ones, as specified in underbraces.

We consider a narrowband packet centered around k_0 of width δk, i.e., $\xi=\delta k/k_0\ll1$. We re-center the modes around k_0 by defining

$$A_q\equiv A_{k-k_0}\equiv\exp[i(\omega_{k_0}+v_g q)t]a_k, \tag{6}$$

where we use the Taylor expansion of the dispersion relation $\omega_k=\omega_{k_0}+v_g q-\Omega q^2+v_3q^3+\cdots$, with $\omega_{k_0}=2\sin\frac{\pi k_0}{N}$, $v_g\equiv2\frac{\pi}{N}\cos\frac{\pi k_0}{N}$, $\Omega\equiv\frac{\pi^2}{N^2}\sin\frac{\pi k_0}{N}$, and $v_3\equiv-\frac{1}{3}\left(\frac{\pi}{N}\right)^3\cos\frac{\pi k_0}{N}$. The evolution of A_q is ruled by

$$\begin{aligned}i\dot{A}_q=&\left[-\Omega q^2A_q+\chi q^3\right]A_q\\&+\sum_{q_1,q_2,q_3}\left[V_0+W_0(q+q_1+q_2+q_3)\right]A_{q_1}^*A_{q_2}A_{q_3}\\&\times\delta(q+q_1-q_2-q_3),\end{aligned} \tag{7}$$

where we neglect non-resonant terms (rotating-wave approximation) and the nonlinear tensor is approximated by the lowest order terms:

$$V_0\equiv\frac{3\beta}{N}\sin^2\frac{\pi k_0}{N}, \tag{8}$$

$$W_0\equiv\frac{3\beta\pi}{4N^2}\sin\frac{2\pi k_0}{N}. \tag{9}$$

If we proceed by defining $\Phi(\theta,t) \equiv \sum_q A_q e^{iq\theta} = \Phi(\theta+2\pi,t)$, we easily obtain, from Eq. (7), that Φ obeys to

$$i\frac{\partial \Phi}{\partial t} = \underbrace{\Omega\frac{\partial^2 \Phi}{\partial \theta^2} + V_0|\Phi|^2\Phi}_{\text{NLSE}} \underbrace{+ i v_3\frac{\partial^3 \Phi}{\partial \theta^3} - 4iW_0|\Phi|^2\frac{\partial \Phi}{\partial \theta}}_{\text{h.o. terms}}, \tag{10}$$

where we recognize (and mark in underbraces) the well-known NLSE equation in the periodic domain $[0,2\pi]$ and two high-order corrections, namely the third-order dispersion and a second nonlinear term, which resembles a nonlinear (depending on $|\Phi|^2$) correction on group-velocity v_g. Similar terms can be found in the hydrodynamics of surface water waves [54,55]. Notice that, for $k_0 = \frac{N}{2}$, the higher-order terms vanish, i.e. $v_3 = W_0 = 0$, and one recovers from Eq. (10) the well-known integrable NLSE.

By introducing $I_0 \equiv \frac{1}{2\pi}\int_0^{2\pi}|\Phi(\theta,t)|^2 d\theta$, i.e., the total intensity (or mass) of the field Φ, and the variables $\tau = \Omega t$ and $\phi = \Phi/I_0^{\frac{1}{2}}$, Eq. (10) becomes

$$i\frac{\partial \phi}{\partial \tau} = \underbrace{\frac{\partial^2 \phi}{\partial \theta^2} + \Lambda|\phi|^2\phi}_{\text{NLSE}} + \underbrace{i\chi\frac{\partial^3 \phi}{\partial \theta^3} - i\Lambda\nu|\phi|^2\frac{\partial \phi}{\partial \theta}}_{\text{h.o. terms}}, \tag{11}$$

The main control parameter is

$$\Lambda \equiv \frac{V_0 I_0}{\Omega} = \frac{3\beta I_0 N}{\pi^2}\sin\frac{\pi k_0}{N} = \frac{3\beta N}{2\pi^2} I_0\omega_{k_0} = \frac{3\beta N}{2\pi^2}E_{k_0}, \tag{12}$$

where we used the definitions above and put $E_{k_0} = I_0\omega_{k_0}$; $\chi \equiv v_3/\Omega$ and $\nu = 4\frac{W_0}{V_0}$.

The basic mechanism that yields interesting dynamical regimes in Eq. (11) is MI. Eq. (11) has a homogeneous (θ-independent) solution $\tilde{\phi}(\tau) = \phi_0 e^{-i\Lambda|\phi_0|^2\tau}$, where ϕ_0 quantifies the wave amplitude. For the sake of definiteness, we take $\phi_0 = 1$. The standard analysis of MI proceeds as follows. We replace the perturbed *Ansatz* $\phi(\theta,\tau) = [1+u(\theta,\tau)+iv(\theta,\tau)]\,e^{-i\Lambda\tau}$ (where u and v are assumed small) in Eq. (11) and linearize the resulting equation. The perturbations are assumed periodic in θ, *i.e.*, $u, v \sim e^{ip\theta}$. It turns out that the MI gain is $g_p = |p|\left(2\Lambda - p^2\right)^{\frac{1}{2}}$. We notice that in this expression χ and ν play no role.

We also notice that MI is found for $p^2 < 2\Lambda$. For p is inherently discrete, no MI is observed if $\Lambda < \frac{1}{2}$, *i.e.*, for $\beta < \frac{\pi^2}{3NE_{k_0}}$. Below this threshold no significant energy exchange occurs between modes, apart from small oscillations due to non-resonant terms, neglected in Eqs. (7). Vice-versa a single mode is unstable for $\frac{1}{2} \le \Lambda < 2$, two modes are unstable for $2 \le \Lambda < \frac{9}{2}$, and so on. These threshold values are related to (generally regular) mode mixing, while the *stochasticity* of β-FPUT can be estimated to happen for $\delta k \sim \Lambda$[45]. The energy exchange between modes is thus expected to be regular for $\beta \ll \beta_0 \equiv \frac{2\pi^2 k_0}{3NE_{k_0}}$, i.e., what we consider here.

We recall that the MI analysis of Eq. (2) gives a more involved result [47,49], which in our notation reads

$$\begin{aligned}
&\left[\tilde{\omega}^2 + \omega_{\text{NL}}^2 + 2(1+2\alpha)\left(\cos\frac{2\pi k_0}{N}\cos\frac{2\pi p}{N} - 1\right)\right.\\
&\qquad\left. -2\alpha\left(\cos\frac{2\pi k_0}{N} - \cos\frac{2\pi p}{N}\right)\right]\\
&\left[\tilde{\omega}^2 + \omega_{\text{NL}}^2 + 2(1+2\alpha)\left(\cos\frac{2\pi k_0}{N}\cos\frac{2\pi p}{N} - 1\right)\right.\\
&\qquad\left. +2\alpha\left(\cos\frac{2\pi k_0}{N} - \cos\frac{2\pi p}{N}\right)\right]\\
&= 4\left[\tilde{\omega}\omega_{\text{NL}} - (1+2\alpha)\sin\frac{2\pi k_0}{N}\sin\frac{2\pi p}{N}\right]^2,
\end{aligned} \tag{13}$$

where $\alpha \equiv \frac{3\beta I_0}{N}\sin^2\frac{\pi k_0}{N} = V_0 I_0$, $\omega_{\text{NL}} = \sqrt{1+\alpha}\omega_{k_0}$ is the nonlinearity-corrected angular frequency, and $\tilde{\omega}(p)$ is the dispersion relation for a perturbation of the pth mode around k_0. If $\tilde{\omega}$ is complex, this yields either an exponential decrease or an increase of perturbations, i.e., the MI gain.

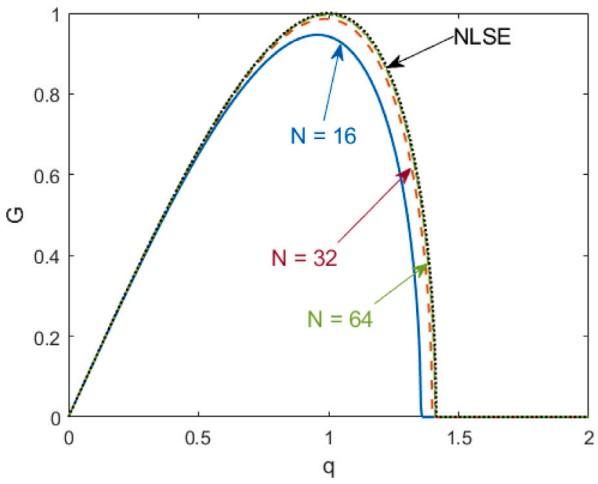

Fig. 1. Comparison of MI gain curves obtained from linearization of Eqs. (2) (blue solid, red dashed and green dash-dotted lines) and (11) (black dotted line). We take $\Lambda = 1$ and $k_0 = \frac{N}{2}$ and different $N = 16, 32, 64$ as labeled inside the figure. (For interpretation of the references to color in this figure legend, the reader is referred to the web version of this article.)

In Fig. 1, we compare the gain obtained from Eq. (13) with the one obtained from Eq. (11) for $\Lambda = 1$ and $k_0 = \frac{N}{2}$. We notice that the MI sidebands (represented as a continuous function of $q > 0$—the sidelobes are symmetric in q) obtained from NLSE (dotted black line) are actually slightly broader and achieve higher maximum gain than those given by Eq. (13). This phenomenon is more and more apparent as N decreases from 64 to 16: notice how the green dash-dotted line is close to the black dotted one, while the red dashed line departs a bit more, and finally for $N = 16$, the blue solid line predicts a significantly (about 10%) smaller gain than the NLSE gain, in a narrower wavenumber range. It is thus apparent that narrow-band approximation leading to Eq. (11) is less accurate for small N. We also verified (results not shown) that, for larger Λ, this discrepancy grows larger.

Our focus here is the behavior of the FPUT chain beyond the initial stage of MI exponential growth. The best known solutions of NLSE with one unstable mode are the Akhmediev breather (AB) that is periodic in space and decays symmetrically in time and the doubly periodic solutions, which exhibit a recurrent behavior in time [5,57]. The recurrence behavior can be characterized by a three-mode truncation [19,52,58], which yields an integrable 1 d.o.f. Hamiltonian system or by a perturbation technique based on the finite-gap method [20,21,53]. The former is more intuitive than the latter and is qualitatively satisfactory, but misses the quantitative parameters of the dynamics (amplitude and period of the periodic solutions) by about 15–20%: it is nevertheless a powerful illustrative tool. Solutions with two unstable modes have been also obtained [59], analyzed in terms of finite-gap theory [20] and preliminarily tested in experiments [60].

We consider a three-wave packet (k_0-1, k_0, k_0+1). We assume that at $\tau = 0$, $|c_0|^2 + |c_1|^2 + |c_{-1}|^2 = 1$. In Ref. [19,52] it was shown that a three-mode truncation of NLSE can be reduced to a 1 d.o.f. Hamiltonian system in terms of canonically conjugate variables $\eta \equiv |c_1|^2 + |c_{-1}|^2$ and $\psi \equiv \frac{\text{Arg}\,c_1 + \text{Arg}\,c_{-1}}{2} - \text{Arg}\,c_0$. Such an approach and the associated phase-plane representation turns out to be beneficial also for generalization of Eq. (11) [61] or Zakharov equation for deep water [62], and even for drawing adequate phase-space pictures of doubly periodic (infinite-modes) solutions [17]. The phase portrait (Hamiltonian level sets) for the NLSE truncation is shown in Fig. 2(a) for $\Lambda = 1$ (i.e., peak gain of the MI band). A double-loop orbit homoclinic to the origin (i.e., a separatrix with figure eight profile) is clearly visible, a behavior common to generic double-well potentials in mechanics.

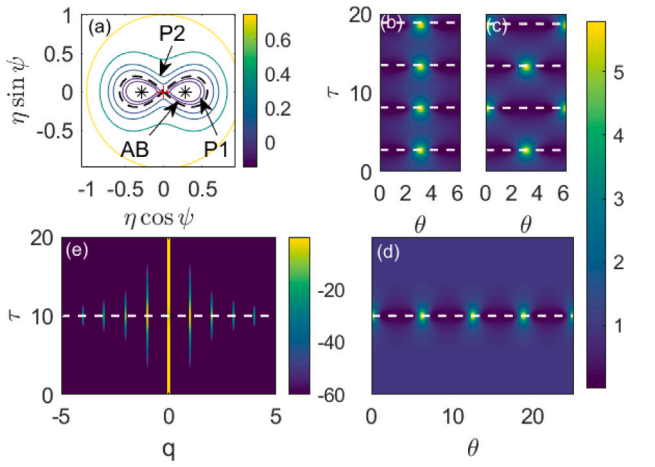

Fig. 2. Summary of NLSE solutions for a single unstable mode. (a) Phase portrait for $\Lambda = 1$, see Ref. [19,52]. (b) False-color plot of the space–time (on the infinite line, for clarity) evolution of $|\phi|^2$ (in linear scale) for a period-1 (P1) solution ($\psi_0 = 0$), inside the separatrix in (a); the dashed lines correspond to the maximum focal points as predicted by finite-gap method; (c) same as (b) for a period-2 (P2) solution ($\psi_0 = \frac{\pi}{2}$), outside the separatrix in (a). (d) same as (b) for the AB, corresponding to the homoclinic orbit in panel (a); the dotted line corresponds to the maximum focusing point, a free parameter of the AB solution. (e) the spatial spectrum corresponding to (d) in dB scale. (For interpretation of the references to color in this figure legend, the reader is referred to the web version of this article.)

We show in Fig. 2(d-e) the evolution in time of the celebrated AB of Eq. (11) ($\chi = \nu = 0$). In the spatial coordinate, Fig. 2(d), we observe the growth of a periodic train of pulses that after reaching the maximal focal point at $\tau = 10$ (dotted line) decays and converges to the homogeneous solution at $\tau \to \infty$. The corresponding spatial spectrum, Fig. 2(e), shows that, to the initial growth of an unstable mode, follows the cascaded generation of its integer multiples mp. The spectrum is maximally broadened at $\tau = 10$ and then the process reverses. All modes are locked with the first and this explains why a single d.o.f. is enough to describe this dynamics. The AB corresponds to the homoclinic orbit (separatrix, i.e., the typical figure eight) in panel (a).

Then, we consider a simple three-modes initial conditions: for simplicity, we assume $c_1 = c_{-1}$ and $\eta_0 \equiv \eta(0) = 0.02$. The evolution of solutions inside ($\psi_0 \equiv \psi(0) = \pi$, which is equivalent to $\psi_0 = 0$) or outside ($\psi_0 = \pi/2$) the separatrix are shown in Fig. 2(b-c), respectively. They correspond to a 0 (π) shift in phase-plane from one recurrence to the next and are denoted as period-1 (P1) or period-2 (P2), respectively. In Refs. [20,21,53], it was shown that starting from the following single unstable mode Ansatz

$$\phi(\theta, 0) = \sqrt{P}\left[1 + \sqrt{2} b e^{i\psi_0} \cos q\theta\right], \tag{14}$$

which corresponds to the present three-mode initial condition if $P = 1 - \eta_0$ and $b = \sqrt{\frac{\eta_0}{P}}$, the first recurrence occurs at time τ_1 and the nth successive at $\tau_1 + n\Delta\tau$, n integer. These quantities, in the limit of small b, read $\tau_1 = \frac{1}{\sigma_1} \log \frac{\sigma_1^2}{2a_0^4|e_+|}$ and $\Delta\tau = \frac{1}{\sigma_1} \log \frac{\sigma_1^4}{4a_0^4|e_+ e_-|}$, where $a_0 \equiv \sqrt{\frac{\Lambda}{2p}}$, $\sigma_1 = \sqrt{4a_0^2 - 1}$ is related to g_p above for $p = 1$, and $e_\pm = -i\sqrt{2\eta_0} \sin\left(\psi_0 \mp \beta_1\right)$, with $\beta_1 = \cos^{-1} \frac{1}{2a_0}$, are the growing and decaying eigenvectors of MI.

These predictions are included in Fig. 2 as dashed lines: it is apparent that they capture almost perfectly the recurrent dynamics. The corresponding spectra (not shown) exhibit the same dynamics of panel (e) at each recurrence cycle, with all secondary modes locked to the first one. The main information is thus carried by the relative phase ψ and it is apparent the 1 d.o.f. nature of the dynamics. Finally, we recall that P1 and P2 solutions can be put in correspondence to doubly periodic solutions [8].

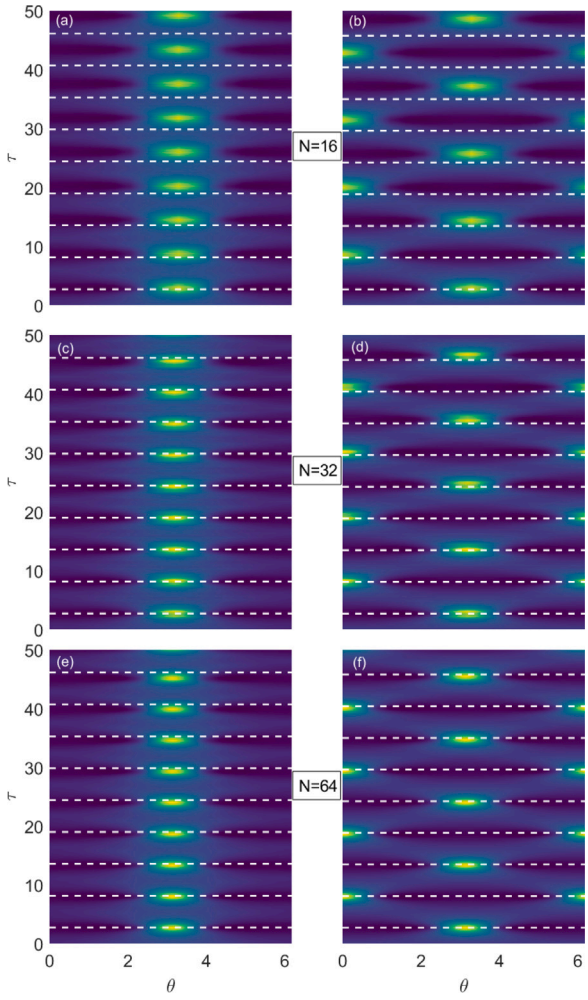

Fig. 3. False-color plots of the space–time evolution of $|\phi|^2$ in Eq. (11) reconstructed from the integration of Eq. (2) with $\Lambda = 1$ and $\eta_0 = 0.02$. (a), (b) $N = 16$, $\beta = 0.0129$; (c), (d) $N = 32$, $\beta = 3.21 \times 10^{-3}$; (e), (f) $N = 64$, $\beta = 8.03 \times 10^{-4}$. (a, c, e) P1 orbits ($\psi_0 = \pi$); (b, d, f) P2 orbits ($\psi_0 = \frac{\pi}{2}$). (For interpretation of the references to color in this figure legend, the reader is referred to the web version of this article.)

This lengthy classification will guide the reader to the interpretation of the numerical results reported in Section 3. More details can be found in the literature, which is still thriving after more than 30 years of work. The goal of this work is to probe the limits of the NLSE approximation of the β-FPUT.

3. Numerical results

We consider as initial conditions the narrowest possible packet $(k_0 - 1, k_0, k_0 + 1)$. We limit ouserselves to $\frac{1}{2} \leq \Lambda < 2$, i.e., a single unstable mode.

We integrate Eq. (2) by using a 6th-order symplectic integrator [63, 64], with integration step $\Delta t = 0.01$ to guarantee the conservation of the Hamiltonian in Eq. (1) within a relative error less than 10^{-10}.

3.1. $k_0 = \frac{N}{2}$

As a first numerical experiment we consider P1 (P2) orbits for $k_0 = N/2$, $I_0 = N$, $\Lambda = 1$, $\psi_0 = \pi$ ($\psi = \frac{\pi}{2}$), and initial sideband fraction $\eta_0 = 0.02$. We integrate up to $\tau = 50$ and reconstruct the NLSE amplitude ϕ, according to the definitions above. Recall that the narrowband approximation is the proper NLSE, see Eq. (11).

In Fig. 3 we show $|\phi|^2$ for $N = 16$ (a,b), $N = 32$ (c,d) and $N = 64$ (e,f): both orbit types behave as expected, although the prediction

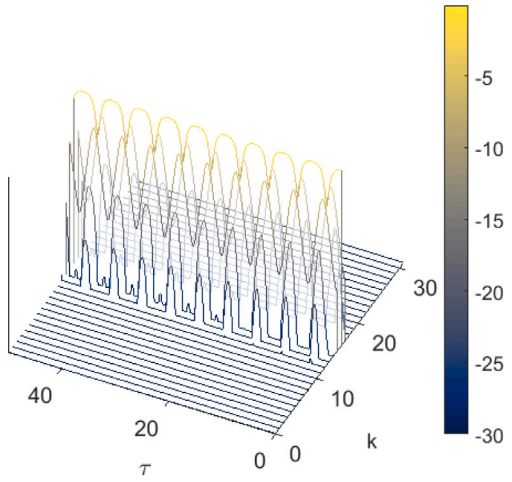

Fig. 4. Evolution in τ of the modal intensities, $|a_k|^2$ in dB, reconstructed from the integration of Eq. (2) with $N = 32$, $\Lambda = 1$, $\eta_0 = 0.02$, and $\psi_0 = 0$ corresponding to a P1 orbit. The surface is semi-transparent to highlight the symmetry around $k_0 = 16$. (For interpretation of the references to color in this figure legend, the reader is referred to the web version of this article.)

of the finite-gap method (dashed white lines) are less accurate for $N = 16$, exhibiting a systematic anticipation of the recurrence τ. For $N = 32$ the accuracy improves; finally for $N = 64$, the dynamics looks indistinguishable from the NLSE-based predictions.

In order to assure the validity of our approximations, we show in Fig. 4 the evolution of $|a_k|^2$ for the example of Fig. 3(c) ($N = 32$, P1 solution). The energy exchange mechanism is apparently very regular and the recurrent behavior exhibits a phase-locking mechanism amongst the modes outside the initial triplet and $a_{k_0\pm1}$, exactly as discussed for Fig. 2. P2 solutions behave in a very similar manner.

3.2. $k_0 \neq \frac{N}{2}$

As k_0 departs from the band edge, nonzero higher-order terms in Eq. (11) appear. While MI is not modified by nonzero χ and ν, the nonlinear evolution can be affected as we show below. We limit ourselves to values of k_0 not far from the band edge since the MI gain drops rapidly as such deviation progressively increases.

In Fig. 5, we keep the same Λ as in Fig. 3, but change k_0. For the sake of brevity we choose it slightly larger (smaller) than $\frac{N}{2}$ for P1 (P2) orbits, which are shown in the left (right) panels. First, we notice that both type of orbits are preserved; second, that the recurrence τ is well predicted by finite-gap theory (with the same inaccuracies for small $N = 16$). The main discrepancy is an almost linear shift in θ of the recurrence points from one focusing event to the next.

While we could resort to a similar analysis as in Ref. [53], we present a simpler explanation. The last term in Eq. (11) ($-i\Lambda\nu|\phi|^2\frac{\partial\phi}{\partial\theta}$) resembles a correction of the group velocity of the wave packet. It can be thus formally eliminated by a (ϕ-dependent) coordinate transform,

$$\theta' = \theta - \Lambda\nu\int_0^\tau \left(|\phi|^2 - |\phi_{\rm BG}|^2\right)\mathrm{d}\tau + \Lambda\nu|\phi_{\rm BG}|^2$$
$$\tau' = \tau, \tag{15}$$

where $|\phi_{\rm BG}|^2$ denotes the background density of the recurring pattern. If we neglect the oscillating part and keep the background only (here $|\phi_{\rm BG}|^2 = 1$), we estimate the linear shift as $\Delta\theta = \Lambda\nu\tau$. This approximation is included in Fig. 5 as dotted red lines. It is apparent that this simple result explains very well the progressive shift in θ that we observe in FPUT simulations. Small deviations occur at large τ and are apparent only for $N = 16, 32$: they can be ascribed to the first order truncation of the nonlinear terms.

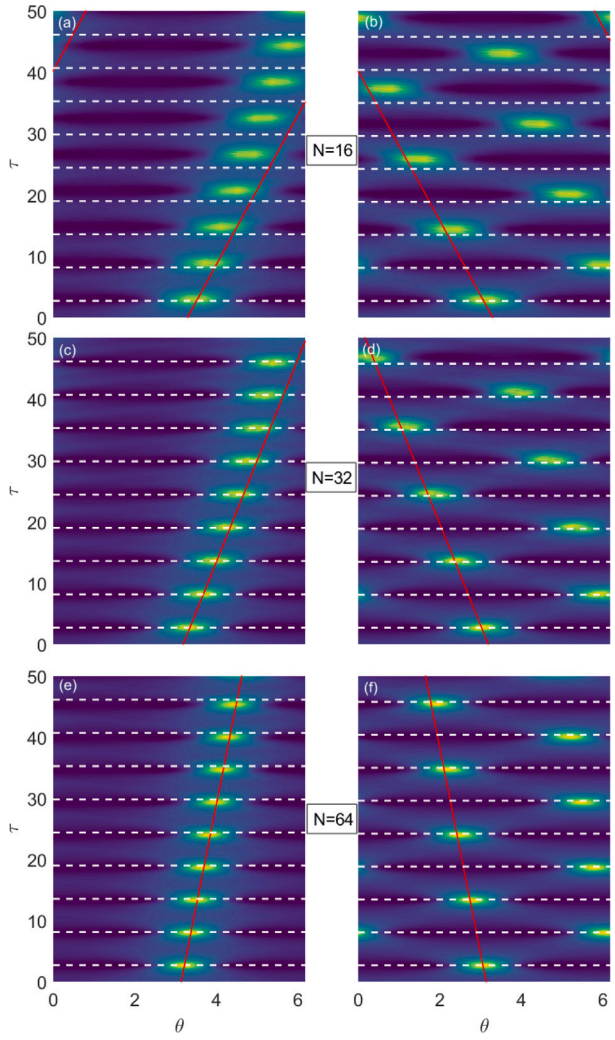

Fig. 5. False-color plots of the space–time evolution of $|\phi|^2$ in Eq. (11) reconstructed from the integration of Eq. (2) with $\Lambda = 1$ and $\eta_0 = 0.02$. (a), (b) $N = 16$, $k_0 = 9(\mathrm{P1}), 7(\mathrm{P2})$, $\beta = 0.0131$; (c), (d) $N = 32$, $k_0 = 19(\mathrm{P1}), 13(\mathrm{P2})$, $\beta = 3.35\times10^{-3}$; (e), (f) $N = 64$, $k_0 = 38(\mathrm{P1}), 26(\mathrm{P2})$, $\beta = 8.39\times10^{-4}$. (a, c, e) P1 orbits ($\psi_0 = \pi$); (b, d, f) P2 orbits ($\psi_0 = \frac{\pi}{2}$). (For interpretation of the references to color in this figure legend, the reader is referred to the web version of this article.)

3.3. Stochasticity layer

At this point, we could hastily state that the NLSE homoclinic structure is well reproduced by the β-FPUT system and higher-order corrections have only a minor impact, as known in water waves [61]. Still, keeping $\Lambda = 1$ and using an intermediate value of ψ_0 (a divergence of the recurrence time can be observed for a specific value, well predicted in Ref. [20], corresponding to the AB, and confirmed in fiber optics experiments [16]), we observe pseudo-stochastic jumps between P2 and P1 orbits (not shown here): this hints at the existence of a stochastic layer that replaces in the β-FPUT the separatrix of the integrable NLSE limit.

This can be observed much more clearly for larger Λ. For instance, we take $\Lambda = 1.5$, $N = 16$, $k_0 = 8$, and integrate up to $\tau = 500$ (corresponding to $t = 1.29\times10^4$). We start with different values of η_0 and map the resulting evolution in the phase-plane defined above and exemplified in Fig. 2(a): the results are summarized in Fig. 6.

In Fig. 6(a), starting from $\psi_0 = \pi$, we expect P1 orbits to occur. This is actually the case. Orbits with larger η_0 are expected to lie inside those with a smaller initial value (i.e., closer to the separatrix): we observe

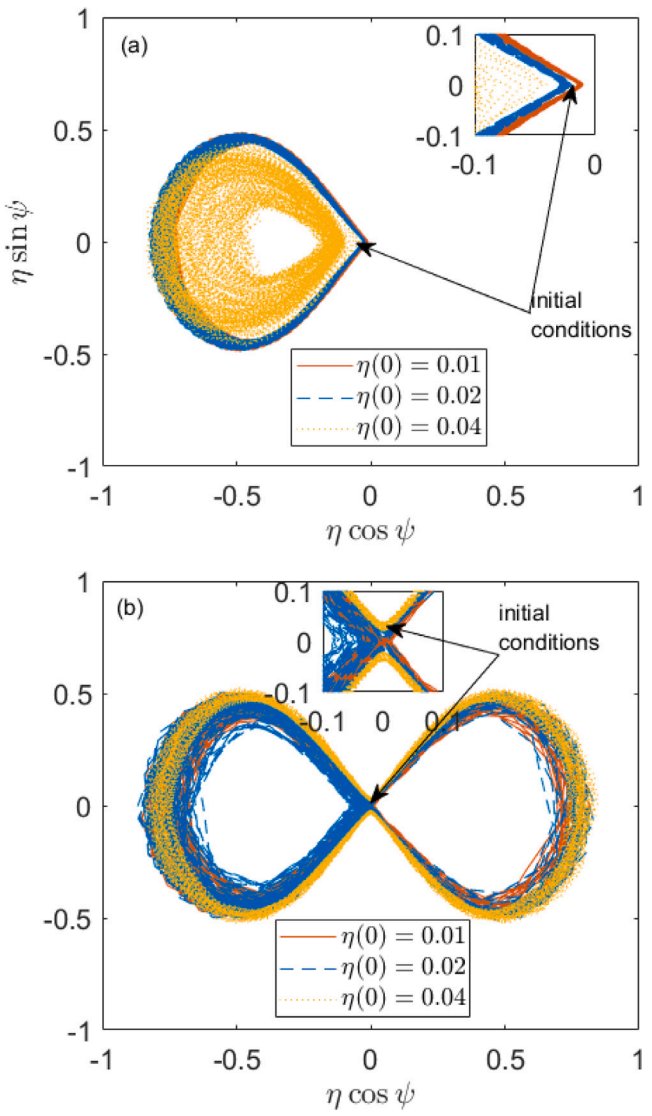

Fig. 6. Phase-plane representation [according to Fig. 2(a)] of the β-FPUT dynamics with $N = 16$ oscillators and $\Lambda = 1.5$. Red solid lines obtained with $\eta_0 = 0.01$; blue dashed lines, $\eta_0 = 0.02$; yellow dotted lines $\eta_0 = 0.04$ (a) $\psi_0 = \pi$ (b) $\psi_0 = \frac{\pi}{2}$. (For interpretation of the references to color in this figure legend, the reader is referred to the web version of this article.)

instead that orbits are irregular and the largest η_0 gives a broadly wandering trajectory that moves away from the separatrix.

The behavior is much more involved when $\psi_0 = \frac{\pi}{2}$, see Fig. 6(b). We would anticipate to observe P2 orbits, which are expected, in general, to be more robust to perturbations [65]. Instead, for $\eta_0 = 0.01, 0.02$ the trajectory jumps from one potential well to the other in a pseudo-stochastic way. Finally it seems to settle in the left-hand potential, but sporadic jumps can still be observed for longer integration times. A slightly larger initial $\eta_0 = 0.04$ allows us to observe a fast oscillating, but persistent, P2 trajectory (look in the inset, the yellow dotted line always stays away from the origin, in contrast to the blue dashed and red solid ones). This value of η_0 for $\psi_0 = \frac{\pi}{2}$ is a rough estimate of the width of the stochastic layer lying outside the separatrix. For $N = 32$, we can observe a similar phenomenon, but for smaller η_0. For $N = 64$, the stochastic layer is much harder to detect. For larger Λ, the effect is even clearer. As, from Eq. (12), $\Lambda \sim \beta N^2$, preliminary results seem to show that the stochastic layer expands almost linearly with β. For the present numerical result is already difficult to interpret, we do not investigate further the case of $k_0 \neq \frac{N}{2}$.

4. Conclusions and perspectives

We numerically investigated the dynamics of β-FPUT chains under the eye of its continuous NLSE approximation. We focused on a single unstable mode, which is equivalent to a single d.o.f. mechanical system, because all other modes are expected to be enslaved to the main one. We find that the two topologically different solutions of the NLSE can be found also in the FPUT simulations, provided a correct mapping of normal modes is defined. The recurrence times are very close to those predicted for NLSE by means of the finite-gap perturbation theory. This applies not only to the edge of the Brillouin zone ($k_0 = \frac{N}{2}$), where higher order terms are negligible, but also close to it. A shift in space is observed, which is shown, from a suitable generalization of the NLSE, to be proportional to the background intensity of the recurring solution. The analytical predictions of recurrence times are almost unaffected by higher-order terms.

Finally, by looking close to the NLSE separatrix, we discover that pseudo-stochastic jumps from outside to inside the separatrix occur (i.e., a P2 orbit erratically starts to behave as P1 orbits). We found that excitation of P1 orbits are seemingly (in the limit of our simulation times) immune to this effect, instead.

Our work represents a different perspective on the regular behavior of the FPUT problem well below the so-called stochasticity threshold, i.e., the chaotic regime, an understudied problem that may provide a fresh view to the long story of the FPUT problem. We also believe that it is safe to identify NLSE recurrence as a manifestation identical to that observed in the β-FPUT problem. For different generalizations of the NLSE apply to many different physical setting, in our opinion, it is not a vocabulary abuse to consider their recurrent behavior in the family of FPUT recurrence phenomena.

CRediT authorship contribution statement

Andrea Armaroli: Writing – review & editing, Writing – original draft, Visualization, Validation, Software, Investigation, Formal analysis, Conceptualization. **Stefano Trillo:** Writing – review & editing, Project administration, Investigation, Funding acquisition, Formal analysis, Conceptualization.

Declaration of competing interest

The authors declare that they have no known competing financial interests or personal relationships that could have appeared to influence the work reported in this paper.

Data availability

Data will be made available on request.

Acknowledgments

We acknowledge the financial support of Italian MUR (Ministero dell'Università e della Ricerca) under grants 2020X4T57A and 2022NCTCY—NextGenerationEU (with the European Union). We thank M. Onorato, P. M. Santini, and F. Coppini for fruitful discussion.

References

[1] Bespalov VI, Talanov VI. Filamentary structure of light beams in nonlinear liquids. Sov Phys JETP Lett 1965;3:471–6.
[2] Benjamin TB, Feir JE. The disintegration of wave trains on deep water part 1. Theory. J Fluid Mech 1967;27(3):417–30.
[3] Zakharov VE, Ostrovsky LA. Modulation instability: The beginning. Phys D 2009;238(5):540–8.
[4] Osborne AR. Nonlinear ocean waves and the inverse scattering transform, vol. 97, Academic Press; 2009.
[5] Akhmediev NN, Korneev VI. Modulation instability and periodic solutions of the nonlinear Schrödinger equation. Theoret and Math Phys 1986;69(2):1089–93.

[6] Akhmediev N, Eleonskii VM, Kulagin N. Exact first-order solutions of the nonlinear Schrödinger equation. Theoret Math Phys 1987;72:809–18.
[7] Peregrine DH, waves Water. Nonlinear Schrödinger equations and their solutions. J Aust Math Soc (Ser B Appl Math) 1983;25(1):16–43.
[8] Conforti M, Mussot A, Kudlinski A, Trillo S, Akhmediev N. Doubly periodic solutions of the focusing nonlinear Schrödinger equation: Recurrence, period doubling, and amplification outside the conventional modulation-instability band. Phys Rev A 2020;101:023843.
[9] Lake BM, Yuen HC, Rungaldier H, Ferguson WE. Nonlinear deep-water waves: theory and experiment. Part 2. Evolution of a continuous wave train. J Fluid Mech 1977;83(1):49–74.
[10] Hasegawa A. Generation of a train of soliton pulses by induced modulational instability in optical fibers. Opt Lett 1984;9(7):288–90.
[11] Nguyen JHV, Luo D, Hulet RG. Formation of matter-wave soliton trains by modulational instability. Science 2017;356(6336):422–6.
[12] Van Simaeys G, Emplit P, Haelterman M. Experimental demonstration of the Fermi-Pasta–Ulam recurrence in a modulationally unstable optical wave. Phys Rev Lett 2001;87(3):033902.
[13] Kimmoun O, Hsu HC, Branger H, Li MS, Chen YY, Kharif C, et al. Modulation instability and phase-shifted Fermi-Pasta–Ulam recurrence. Sci Rep 2016;6(1):28516.
[14] Mussot A, Naveau C, Conforti M, Kudlinski A, Copie FF, Szriftgiser P, et al. Fibre multi-wave mixing combs reveal the broken symmetry of Fermi-Pasta–Ulam recurrence. Nature Photonics 2018;12(5):303–8.
[15] Pierangeli D, Flammini M, Zhang L, Marcucci G, Agranat AJ, Grinevich PG, et al. Observation of Fermi-Pasta–Ulam-Tsingou recurrence and its exact dynamics. Phys Rev X 2018;8(4):41017.
[16] Naveau C, Szriftgiser P, Kudlinski A, Conforti M, Trillo S, Mussot A. Experimental characterization of recurrences and separatrix crossing in modulational instability. Opt Lett 2019;44(22):5426–9.
[17] Vanderhaegen G, Szriftgiser P, Naveau C, Kudlinski A, Conforti M, Trillo S, et al. Observation of doubly periodic solutions of the nonlinear Schrödinger equation in optical fibers. Opt Lett 2020;45(13):3757–60.
[18] Vanderhaegen G, Naveau C, Szriftgiser P, Kudlinski A, Conforti M, Mussot A, et al. Extraordinary modulation instability in optics and hydrodynamics. Proc Natl Acad Sci USA 2021;118:e2019348118.
[19] Trillo S, Wabnitz S. Dynamics of the nonlinear modulational instability in optical fibers. Opt Lett 1991;16(13):986–8.
[20] Grinevich PG, Santini PM. The exact rogue wave recurrence in the NLS periodic setting via matched asymptotic expansions, for 1 and 2 unstable modes. Phys Lett A 2018;382(14):973–9.
[21] Grinevich PG, Santini PM. The finite gap method and the analytic description of the exact rogue wave recurrence in the periodic NLS Cauchy problem. 1. Nonlinearity 2018;31(11):5258–308.
[22] Ercolani N, Forest M, McLaughlin DW. Geometry of the modulational instability: III. Homoclinic orbits for the periodic sine-Gordon equation. Physica D 1990;43(2):349–84.
[23] Trillo S, Wabnitz S. Nonlinear modulation of coupled waves in birefringent optical fibers. Phys Lett A 1991;159(4):252–6.
[24] Conforti M, Armaroli A, Kudlinski A, Mussot A, Rota Nodari S, Dujardin G, et al. Heteroclinic structure of parametric resonance in the nonlinear Schrödinger equation. Phys Rev Lett 2016;117(1):013901.
[25] Fermi E, Pasta JR, Ulam S. Study of Nonlinear Problems. Tech. Rep. LA-1940, Los Alamos Scientific Lab., N. Mex; 1955.
[26] Akhmediev NN. Déjà vu in optics. Nature 2001;413:267–8.
[27] Vanderhaegen G, Szriftgiser P, Kudlinski A, Conforti M, Trillo S, Droques M, et al. Observation of four Fermi-Pasta–Ulam-Tsingou recurrences in an ultra-low-loss optical fiber. Opt Express 2020;28(12):17773.
[28] Infeld E. Quantitive theory of the Fermi-Pasta–Ulam recurrence in the nonlinear Schrödinger equation. Phys Rev Lett 1981;47(10):717–8.
[29] Akhmediev NN, Ankiewicz A. Modulation instability, Fermi-Pasta–Ulam recurrence, rogue waves, nonlinear phase shift, and exact solutions of the Ablowitz-Ladik equation. Phys Rev E 2011;83(4):046603.
[30] Soto-Crespo JM, Ankiewicz A, Devine N, Akhmediev N. Modulation instability, cherenkov radiation, and Fermi-Pasta-Ulam recurrence. J Opt Soc Am B 2012;29(8):1930–6.
[31] Kuznetsov EA. Fermi–Pasta–Ulam recurrence and modulation instability. JETP Lett 2017;105(2):125–9.
[32] Ford J. The Fermi-Pasta–Ulam problem: Paradox turns discovery. Phys Rep 1992;213(5):271–310.
[33] Dauxois T, Peyrard M, Ruffo S. The Fermi-Pasta–Ulam 'numerical experiment': History and pedagogical perspectives. Eur J Phys 2005;26(5):3–11.
[34] Berman GP, Izrailev FM. The Fermi–Pasta–Ulam problem: Fifty years of progress. Chaos 2005;15(1):015104.
[35] Zabusky NJ. Fermi–Pasta–Ulam, solitons and the fabric of nonlinear and computational science: History, synergetics, and visiometrics. Chaos 2005;15(1):015102.
[36] Dauxois T, Ruffo S. Fermi-Pasta-Ulam nonlinear lattice oscillations. Scholarpedia 2008;3(8):5538.
[37] Zabusky NJ, Kruskal MD. Interaction of solitons in a collisionless plasma and the recurrence of initial states. Phys Rev Lett 1965;15(6):240–3.
[38] Chirikov BV. A universal instability of many-dimensional oscillator systems. Phys Rep 1979;52(5):263–379.
[39] Livi R, Pettini M, Ruffo S, Sparpaglione M, Vulpiani A. Equipartition threshold in nonlinear large hamiltonian systems: The Fermi-Pasta-Ulam model. Phys Rev A 1985;31:1039–45.
[40] Flach S, Ivanchenko MV, Kanakov OI. q-Breathers and the Fermi-Pasta-Ulam problem. Phys Rev Lett 2005;95:064102.
[41] Onorato M, Vozella L, Proment D, Lvov Y. Route to thermalization in the α-Fermi–Pasta–Ulam system. Proc Natl Acad Sci USA 2015;112:4208–13.
[42] Lvov YV, Onorato M. Double scaling in the relaxation time in the β -Fermi-Pasta–Ulam-Tsingou model. Phys Rev Lett 2018;120(14):144301.
[43] Pace SD, Campbell DK. Behavior and breakdown of higher-order Fermi-Pasta–Ulam-Tsingou recurrences. Chaos 2019;29(2):023132.
[44] Onorato M, Lvov Y, Dematteis G, Chibbaro S. Wave turbulence and thermalization in one-dimensional chains. Phys Rep 2023;1040:1–36, wave Turbulence and thermalization in one-dimensional chains.
[45] Berman GP, Kolovskii AR. The limit of stochasticity for a one-dimensional chain of interacting oscillators. Sov Phys—JETP 1984;60:1116–21.
[46] Zabusky NJ, Deem GS. Dynamics of nonlinear lattices I. Localized optical excitations, acoustic radiation, and strong nonlinear behavior. J Comp Phys 1967;2(2):126–53.
[47] Burlakov VM, Darmanyan SA, Pyrkov VN. Modulation instability and recurrence phenomena in anharmonic lattices. Phys Rev B 1996;54:3257–65.
[48] Burlakov VM, Darmanyan SA, Pyrkov VN. Modulation instability of traveling waves in Fermi-Pasta-Ulam lattices. JETP 1996;81:496–501.
[49] Dauxois T, Khomeriki R, Piazza F, Ruffo S. The anti-FPU problem. Chaos 2005;15(1):015110.
[50] Dauxois T, Khomeriki R, Ruffo S. Modulational instability in isolated and driven Fermi-Pasta-Ulam lattices. Eur Phys J Spec Top 2007;147:3–23.
[51] Pistone L, Chibbaro S, Bustamante MD, Lvov YV, Onorato M. Universal route to thermalization in weakly-nonlinear one-dimensional chainsy. Math Eng 2019;1(4):672–98.
[52] Cappellini G, Trillo S. Third-order three-wave mixing in single-mode fibers: exact solutions and spatial instability effects. J Opt Soc Am B 1991;8(4):824–38.
[53] Coppini F, Grinevich PG, Santini PM. Effect of a small loss or gain in the periodic nonlinear Schrödinger anomalous wave dynamics. Phys Rev E 2020;101(3):1–8.
[54] Dysthe KB. Note on a modification to the nonlinear Schrodinger equation for application to deep water waves. Proc R Soc A 1979;369(1736):105–14.
[55] Lo EY, Mei CC. A numerical study of water-wave modulation based on a higher-order nonlinear Schrodinger equation. J Fluid Mech 1985;150(1985):395–416.
[56] Onorato M. Personal communication. 2023.
[57] Akhmediev NN, Eleonskii VM, Kulagin NE. Generation of periodic trains of picoseconld pulses in an optical fiber: exact solutions. Sov Phys—JETP 1985;62(5):894.
[58] Bivins RL, Metropolis N, Pasta JR. Nonlinear coupled oscillators: Modal equation approach. J Comput Phys 1973;12(1):65–87.
[59] Kedziora DJ, Ankiewicz A, Akhmediev NN. Second-order nonlinear Schrödinger equation breather solutions in the degenerate and rogue wave limits. Phys Rev E 2012;85(6):1–9.
[60] Naveau C, Vanderhaegen G, Szriftgiser P, Martinelli G, Droques M, Kudlinski A, et al. Heterodyne optical time domain reflectometer combined with active loss compensation: A practical tool for investigating Fermi pasta Ulam recurrence process and breathers dynamics in optical fibers. Front Phys 2021;9(April):1–15.
[61] Armaroli A, Brunetti M, Kasparian J. Recurrence in the high-order nonlinear Schrödinger equation: A low-dimensional analysis. Phys Rev E 2017;96(1):012222.
[62] Andrade D, Stuhlmeier R. The nonlinear Benjamin–Feir instability – hamiltonian dynamics, discrete breathers and steady solutions. J Fluid Mech 2023;958:A17.
[63] Yoshida H. Construction of higher order symplectic integrators. Phys Lett A 1990;150(5–7):262–8.
[64] Mauger F. Symplectic leap frog scheme 1.1.0.0. 2013, www.mathworks.com/matlabcentral/fileexchange/38652-symplectic-leap-frog-scheme.
[65] Vanderhaegen G, Szriftgiser P, Kudlinski A, Conforti M, Armaroli A, Mussot A. Observation of the noise-driven thermalization of the Fermi-Pasta–Ulam-Tsingou recurrence in optical fibers. Phys Rev A 2022;106(3):033519.